

PACS numbers: 52.38.Ph; 79.20.Eb; 82.80.–d
DOI: 10.1070/QE2012v042n07ABEH014739

Physics of selective evaporation of components during laser ablation of stainless steels

S.M. Pershin, V.N. Lednev, D.E. Bogatkin, T.A. Labutin, A.F. Bunkin

Abstract. **A physical mechanism of the deviation of plasma composition from stoichiometry during laser ablation of multicomponent alloys is proposed and experimentally verified. This mechanism takes into account the difference in the work functions of the alloy components in the heating–melting–evaporation cycle and makes it possible to take into account selective evaporation when determining the composition of four-component bronzes and substantiate conservation of stoichiometry when analysing the composition of stainless steels. The proposed mechanism of selective evaporation allows one to improve precision of the analysis for multicomponent alloys without reference calibration, which increases the practical importance of the calibration-free laser-induced breakdown spectroscopy (CF LIBS).**

Keywords: *laser ablation, laser plasma, selective evaporation, compositional analysis.*

1. Introduction

Since the discovery of first lasers laser radiation has been used for chemical analysis, matching applications and low-temperature plasma formation [1, 2]. The first studies on the use of lasers to deposit coatings showed that laser evaporation of multicomponent targets may result in deposition of thin films with a complex composition [3]. It was found in the subsequent studies that during laser ablation of samples of complex composition (superconductors, bronzes, etc.) the component ratio in a deposited coating does not always correspond to that for the initial sample [4]. As a result, one must choose appropriate experimental conditions (change the target composition, perform evaporation in an atmosphere of specially chosen gas, etc.) to obtain a coating of specified composition. Laser radiation is also used for sampling and forming laser plasma with subsequent analysis of its composition or the composition of its products [5, 6]. To provide analysis, the laser plasma composition must reflect the sample stoichiometry and exclude the influence of selective evaporation of its components. Unfortunately, this cannot be achieved in practice. To reduce the influence of the sample composition on the results of analysis based on laser sampling methods (laser-induced breakdown spectroscopy, inductively-coupled plasma mass-spectrometry and inductively-coupled plasma atomic-emission spectroscopy with laser sampling) reference samples (standards) are applied for calibration. Sometimes correction methods are used with additionally measured signals, which characterise laser plasma [7]. However, in some cases, where selective evaporation is pronounced (bronzes, nonferrous alloys), the sample composition cannot be analysed [8, 9].

It was previously established [10, 11] that the degree of change in the ratio components in plasma is determined by both the properties of laser radiation and the sample nature. Selective evaporation was revealed for laser radiation wavelengths from 246 nm to 10 μm, energy densities $0.1–10^3$ J cm^{-2} on the target surface, and pulse widths from 120 fs to 100 ns [9, 12, 13]. It was shown in [14] that a reduction of the laser pulse width and laser wavelength, as well as an increase in the power density, reduce deviation from stoichiometry. Nevertheless, it was found that stoichiometry cannot be retained for some samples (bronzes, glasses) even when optimal laser sources are used: the component ratios in the plasma and in the original sample are different.

The calibration-free method of laser-induced breakdown spectroscopy has been widely spread in the last decade [15]. As was believed by its authors [16, 17], composition can be analysed without reference samples if the following requirements are satisfied: (i) plasma is optically thin, (ii) plasma is in local thermodynamic equilibrium, and (iii) the component ratio is the same in the plasma and sample (i.e., stoichiometry is retained). One can check experimentally the validity of the first two requirements or choose detection conditions (spectral lines, delay time with respect to the laser pulse) under which these requirements are satisfied. Generally stoichiometry conservation is not checked and assumed to be always retained. In some cases this holds true (the components of sample additives have similar properties and the content of the sample base exceeds 90%); however, this condition cannot be fulfilled for some samples (bronzes, nonferrous alloys) [8, 18]. The calibration-free laser-induced breakdown spectrosciopy (CF LIBS) gave correct results for gases whose stoichiometry did not change as a result of optical breakdown [19].

A model describing deviation from stoichiometry during laser evaporation was proposed for the first time in [10]; it was shown by the example of bronze samples that the correction of spectra using the proposed model improves the analysis results. In the subsequent studies [20, 21] this approach was used to analyse the spectra of plasma treated in different modes, including one- and two-pulse ones, and for alloys of other types.

S.M. Pershin, V.N. Lednev, A.F. Bunkin Wave Research Center, A.M. Prokhorov General Physics Institute, Russian Academy of Sciences, ul. Vavilova 38, 119991 Moscow, Russia; e-mail: lednev@kapella.gpi.ru;
D.E. Bogatkin, T.A. Labutin Department of Chemistry, M.V. Lomonosov Moscow State University, Vorob'evy gory, 119991 Moscow, Russia

Received 30 September 2011
Kvantovaya Elektronika **42** (7) 605–611 (2012)
Translated by Yu.P. Sin'kov

In this paper, we report the results of studying the influence of selective evaporation on the analysis of the composition of stainless steels during laser ablation.

2. Deviation from stoichiometry during laser evaporation of material

Both direct (optical emission spectroscopy, mass spectroscopy) and indirect (X-ray photoelectron spectroscopy, secondary-ion mass spectrometry, X-ray fluorescence spectroscopy) methods are used to determine the deviation from stoichiometry during laser evaporation of materials.

When using optical emission spectroscopy, the deviation from stoichiometry is found from the ratios of spectral line intensities for different elements in plasma. Generally, the elemental composition of laser plasma is determined by the CF LIBS [17] and compared with the known sample composition. On the assumption of optically thin plasma in local thermodynamic equilibrium, the following expression holds true:

$$I_i^{pk} = A_i^{pk} g_p h\nu_i^{pk} n_i F \frac{\exp(-E_i^p/kT)}{Z_i}, \quad (1)$$

where I_i^{pk} is the line intensity of the $p-k$ electronic transition for the ith particle (in rel. units); A_i^{pk} is the Einstein coefficient for this transition (s^{-1}); g_p is the statistical weight of the pth level; h is Planck's constant; ν_i^{pk} is the $(p-k)$-transition frequency (s^{-1}); n_i is the amount of the ith component in the plasma (mol); Z_i is the partition function at a temperature T; E_i^p is the energy of the pth level (eV); k is the Boltzmann constant; T is temperature (K); and F is an experimental constant (it depends on the experimental scheme, efficiency of plasma emission collection, etc.), which is determined in the procedure of CF LIBS.

One can check experimentally if plasma is optically thin for a given line or record spectra at instants when this condition is obviously implemented. For example, to satisfy this condition, one can record nonresonant lines or lines with a lower level spaced from the ground level by several tenths of an electronvolt [22]. In some cases, the degree of self-absorption of a line can be estimated from its profile [23] or from the intensity ratio for lines with different energies of the lower levels involved in the corresponding transitions [24]. The presence of local thermodynamic equilibrium is checked by comparing the electron temperatures for particles of different types (atoms and ions of different elements) [22]. The coincidence of these temperatures (found from the spectrum) indicates local thermodynamic equilibrium.

The deviation from stoichiometry during laser evaporation of a multicomponent sample is estimated from ratio (1) by expressing the amounts of materials in terms of mass fractions C_i (%) of the ith components in the initial sample and the mass of evaporated materials m:

$$n_i = C_i m/M_i,$$

where M_i is the molar mass (g mol^{-1}) of the ith component. After substituting these expressions into formula (1), introducing a new constant F' ($F' = Fhm$), and finding the logarithm, we obtain

$$\ln\left(\frac{I_i^{pk}}{A_i^{pk} g_p \nu_i^{pk}}\right) = \ln\left(F' \frac{C_i}{Z_i M_i}\right) - \frac{E_i^p}{kT}. \quad (2)$$

The dependence $I_i^{pk}(E_i^p)$ in the coordinates $\ln[I_i^{pk}/(A_i^{pk} g_p \nu_i^{pk})]$ and E_i^p is plotted for several lines of the same atom, and the temperature is calculated from its slope. The free term $b_i = \ln[F'C_i/(Z_i M_i)]$ is determined for each straight line. Then the material balance condition

$$\sum_i C_i = \frac{1}{F'} \sum_i (Z_i M_i \exp b_i) = 1 \quad (3)$$

is used to calculate the experimental constant F' and then determine the content of each component:

$$C_i = \frac{1}{F'} Z_i M_i \exp b_i. \quad (4)$$

Note that, since the plasma temperature is generally fairly high (up to 10 000 K) and the ionisation energies are different for atoms of different elements, one must take into account the ionisation equilibrium state to correctly determine the plasma composition. To this end, the Saha equation [25] is used:

$$\frac{N_e n^s}{n^{s-1}} = \frac{2Z^s(T)}{Z^{s-1}(T)} \left(2\pi \frac{m_e kT}{h^2}\right)^{3/2} \exp\left(-\frac{E_\infty^{s-1} - \Delta E_\infty^{s-1}}{kT}\right), \quad (5)$$

where N_e is the electron concentration (cm^{-3}); n^s is the amount of s-type ions (mol); m_e is the electron mass; E_∞^{s-1} is the ionisation energy of $s-1$ ions (eV); and ΔE_∞^{s-1} (eV) is the correction to the ionisation energy that takes into account the interaction of ions with plasma. The electron concentration is determined by different methods; generally, Stark line broadening is used to this end [22]. Then the ratio of numbers of atoms and ions is calculated at the known temperature. To find the total amount of a given element in plasma, it is sufficient to take into account only atoms and singly charged ions, because the fraction of doubly charged ions at laser plasma temperatures (up to 10 000 K) is less than 0.01 %. After determining the fraction of ions from (5), the correction factor $\beta_i = 1 + n_i^s/n_i^{s-1}$ is introduced into Eqn (3) by replacing C_i with $\beta_i C_i$ on the left-hand side, and the plasma composition is found.

The deviation from stoichiometry is estimated by comparing the calculated plasma composition with the known sample composition.

3. Model of deviation from stoichiometry during laser evaporation of alloys

The mechanism proposed was described in detail in [10, 21] and we will only briefly consider it here. Laser irradiation of a solid results in its melting; evaporation; and then optical breakdown of the vapor, which leads to the formation of laser plasma. It was shown that in the case of laser breakdown of molecular gases the laser plasma and gas have identical compositions; therefore, one should expect deviation from stoichiometry in the stages preceding the optical breakdown [19]. As was suggested in [10, 21], deviation from stoichiometry during laser ablation of solids occurs in the melting and evaporation stages.

It was experimentally found that the deviation from stoichiometry during laser evaporation is maximum for the samples whose components have significantly different melting and evaporation temperatures and energies. Bronze samples were used to show that the components characterised by lower melting temperatures and heats of fusion and lower evaporation heats and temperatures have a higher concentration in the

plasma after breakdown [9]. For pure materials the evaporated-material mass is known to be inversely proportional to the melting temperature, heat of fusion, and evaporation temperature and heat [26].

It is physically clear that an increase in the melt exposure time to laser radiation before optical breakdown should facilitate selective evaporation. On the contrary, one should expect reduction of this time [for example, when short (pico- or femtosecond) pulses are used] to weaken the manifestation of selective evaporation. Note that the possibility of existence of a metal melt in the superheated state was predicted by L.D. Landau and Ya.B. Zel'dovich [27]. They showed that the high surface tension coefficient of metals can provide a significant metal overheating (up to temperatures exceeding the boiling temperature) and cause a metal–insulator transition. This effect was found for metallic mercury as a conductivity jump upon continuous heating to the critical transition temperature [28].

It is noteworthy that this effect was found during laser-induced plasma formation on a metal surface by Prokhorov et al. [29]. They showed that the metal–insulator transition is accompanied by the generation of a transparency wave in the melt upon laser heating. Boiling does not develop under these conditions, and the laser energy reaches the crater bottom and the metal–melt interface to be spent on melting, which increases the melt lifetime and enhances selective evaporation. The formation of plasma in the optical breakdown region is accompanied by its fast expansion (during the laser pulse) with a shock effect on the melt, as a result of which the latter overflows the crater [30]. Thus, the surface composition does not change (which would occur as a result of solidification of melt with a changed composition), and each new pulse interacts with the fresh surface of purified crater.

During laser evaporation by a nanosecond pulse the depth at which energy dissipates during the pulse (due to the thermal conductivity) is small: less than 1 μm [2]. Let us write the material-balance equation for a pure material, neglecting the energy loss due to the thermal conductivity:

$$n^{\mathrm{gas}} = E_0 A / [c_{\mathrm{sol}}(T_{\mathrm{melt}} - T_{\mathrm{room}}) + \Delta H_{\mathrm{melt}} + c_{\mathrm{liq}}(T_{\mathrm{ev}} - T_{\mathrm{melt}}) + \Delta H_{\mathrm{ev}} + c_{\mathrm{gas}}(T - T_{\mathrm{ev}})], \quad (6)$$

where n^{gas} is the amount of evaporated material (mol); E_0 is the laser pulse energy (mJ); A is a coefficient characterising the laser radiation absorption efficiency of the material; c_{sol}, c_{liq}, and c_{gas} are the specific heats of the material in the solid, liquid, and gaseous states, respectively (J mol^{-1} K^{-1}); T_{melt} is the melting temperature (K); T_{room} is the sample temperature prior to laser irradiation (K); ΔH_{melt} is the melting enthalpy (J mol^{-1}); T_{ev} is the evaporation temperature (K); ΔH_{ev} is the evaporation enthalpy (J mol^{-1}); and T is the temperature (K) at which the vapor undergoes optical breakdown.

During laser ablation target material starts evaporating when the melting temperature T_{melt} is reached and stops with the optical breakdown onset. The time profile of a nanosecond laser pulse is generally described by a Gaussian. When the density power sufficient for melting is reached, the melt begins to intensively evaporate; the evaporation rate increases when approaching the boiling temperature. Components with lower melting and boiling temperatures evaporate more actively and for a longer time. To take into account the influence of this process on selective evaporation, we will transform expression (6) by introducing phenomenologically a factor T/T_{melt}:

$$n^{\mathrm{pl}} = (T/T_{\mathrm{melt}})E_0 A / [c_{\mathrm{sol}}(T_{\mathrm{melt}} - T_{\mathrm{room}}) + \Delta H_{\mathrm{melt}} + c_{\mathrm{liq}}(T_{\mathrm{ev}} - T_{\mathrm{melt}}) + \Delta H_{\mathrm{ev}} + c_{\mathrm{gas}}(T - T_{\mathrm{ev}})], \quad (7)$$

where n^{pl} is the amount of evaporated material in the plasma.

The temperature at which optical breakdown occurs depends on the properties of target material (ionisation energy of atoms in the gas phase, etc.), external factors (buffer gas type and pressure, etc.), and the laser radiation parameters (wavelength and power density on the target surface).

The introduced factor T/T_{melt} is proportional to the active evaporation time of each alloy component from the instant when the melt temperature reaches the T_{melt} value to the temperature T at which selective evaporation is interrupted (for example, at optical breakdown).

In the case of a multicomponent alloy the previous expression can be written for the ith component in the form

$$n_i^{\mathrm{pl}} = (n_i^{\mathrm{sol}}/n)(T/T_{\mathrm{melt}})E_0 A / [c_{i\mathrm{sol}}(T_{i\mathrm{melt}} - T_{\mathrm{room}}) + \Delta H_{i\mathrm{melt}} + c_{i\mathrm{liq}}(T_{i\mathrm{ev}} - T_{i\mathrm{melt}}) + \Delta H_{i\mathrm{ev}} + c_{i\mathrm{gas}}(T - T_{i\mathrm{ev}})], \quad (8)$$

where n_i^{sol} is the amount of the ith material in the solid phase (mol); $n = \sum n_i^{\mathrm{sol}}$.

Let us denote the part of expression (8) where all thermodynamic parameters refer to the ith component as W_i and call it the 'work function':

$$W_i = T_{i\mathrm{melt}}[c_{i\mathrm{sol}}(T_{i\mathrm{melt}} - T_{\mathrm{room}}) + \Delta H_{i\mathrm{melt}} + c_{i\mathrm{liq}}(T_{i\mathrm{ev}} - T_{i\mathrm{melt}}) + \Delta H_{i\mathrm{ev}} + c_{i\mathrm{gas}}(T - T_{i\mathrm{ev}})]. \quad (9)$$

Therefore, the amount of the ith component in the plasma before optical breakdown can be written as

$$n_i^{\mathrm{pl}} = \frac{n_i^{\mathrm{sol}}}{n}\frac{E_0 A T}{W_i} = \frac{C_i m}{M_i n}\frac{E_0 A T}{W_i}, \quad (10)$$

where m is the evaporated mass of the sample; C_i is the ith-component concentration; and M_i is the molar mass.

Correspondingly, the ratio of components i, j, and h in the solid sample can be written as

$$n_i^{\mathrm{sol}}:n_j^{\mathrm{sol}}:n_h^{\mathrm{sol}} = \frac{m_i^{\mathrm{sol}}}{M_i}:\frac{m_j^{\mathrm{sol}}}{M_j}:\frac{m_h^{\mathrm{sol}}}{M_h} = \frac{C_i}{M_i}:\frac{C_j}{M_j}:\frac{C_h}{M_h}. \quad (11)$$

According to (10), the component ratio in the plasma is determined by the following equation [which differs from (11)]:

$$n_i^{\mathrm{pl}}:n_j^{\mathrm{pl}}:n_h^{\mathrm{pl}} = \frac{C_i}{M_i W_i}:\frac{C_j}{M_j W_j}:\frac{C_h}{M_h W_h}. \quad (12)$$

Thus, the component ratios in the plasma differ from the similar ratios for the sample by the factors $W_{i,j,h}$ (work functions). In the case of multicomponent samples, which exhibit deviation from stoichiometry during laser evaporation, the consideration of the work function should make the results of analysis be consistent with the known data for a solid sample.

Therefore, when calculating the sample composition with allowance for selective evaporation, one must use the following expression instead of (1):

$$I_i^{pk} = A_i^{pk} g_p h\nu_i^{pk} F \frac{C_i}{M_i W_i}\frac{\exp(-E_i^p/kT)}{Z_i}. \quad (13)$$

The previously proposed model was checked on samples characterised by deviation from stoichiometry during laser evaporation (bronzes and aluminum-based alloys); its application made analysis more accurate. Our purpose was (i) to analyse the deviation from stoichiometry for steel samples with alloy steels (there are suggestions in the literature that the deviation from stoichiometry for such samples should not be very pronounced; however, there are no experimental data confirming this suggestion) and (ii) to verify the model proposed in the case of weak deviation from stoichiometry during laser evaporation.

4. Experimental

A schematic of the experimental setup is shown in Fig. 1. A pulsed solid-state Nd:YAG laser (1064 nm, 10 ns, 6 mJ pulse^{-1}, 1 Hz) was used for target evaporation. The laser beam was focused on the sample surface by a lens (f = 80 mm). To improve the reproducibility and reduce the influence of crater formation on the ablation, the focused-beam waist was located at a depth of 1 mm from the sample surface. The spot diameter on the sample surface was found from the crater diameter (measured per pulse) to be 120 μm, a value corresponding to an average power density of 5.5×10^9 W cm^{-2}. An image of the laser plasma on the 1 : 1 scale was projected (using a quartz lens) onto the input slit of the spectrograph. The plasma plume was oriented along the slit, the width and height of which were 50 μm and 4 mm, respectively. A Shamrock Andor spectrograph was equipped with a detector based on an intensified CCD (Andor iStar). The parameters of the entire system were as follows: spectral resolution 0.1 nm, time resolution 10 ns, spectral range 200–800 nm, and spectral detection window 18 nm. To check the validity of condition for local thermodynamic equilibrium, we recorded a spectrum from a small central region in the plasma, which provided the maximum intensity of iron lines during the first 2 μs of plasma luminescence. The horizontal size of the image of the region under study was set by the width of the spectrograph slit (50 μm). The vertical size of the slit was 4 mm, and several rows of pixels were chosen in the obtained image on the CCD matrix, thus setting the vertical size of the region under consideration (300 μm).

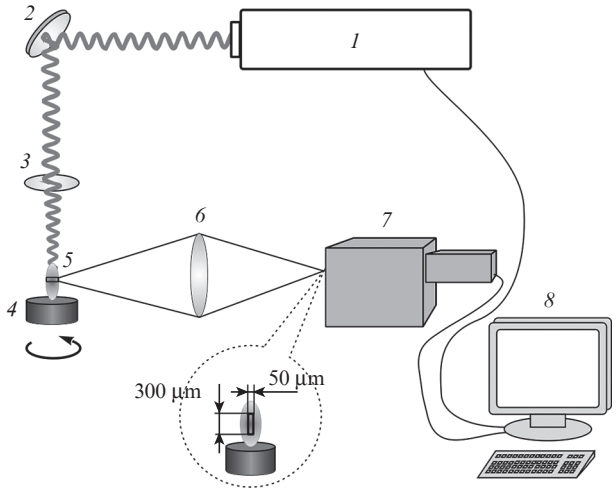

Figure 1. Schematics of the experimental setup: (*1*) Nd:YAG laser (1064 nm, 10 ns, 6 mJ pulse^{-1}, 1 Hz), (*2*) mirror, (*3*) focusing lens (f = 80 mm), (*4*) sample, (*5*) plasma, (*6*) projecting lens (quartz, f = 80 mm), (*7*) spectrograph equipped with an intensified CCD, and (*8*) control PC; the inset shows a projection of the laser plasma image on the input slit of the spectrograph.

The objects of study were samples of stainless steel with high nickel and chromium contents. The samples were prepared and certified at the German Institute for Standardisation (Berlin). These samples were chosen because ferrous alloys (with an iron content exceeding 95%) do not exhibit any deviations from stoichiometry during laser evaporation. At the same time, there is no information in the literature about the degree of deviation from stoichiometry during laser evaporation for stainless steels with a high (more than 20%) content of other components. Before measurements the samples were polished by a grinding paper to reduce the surface roughness and thus improve the reproducibility of ablation conditions. The sample composition is given in Table 1.

Table 1. Compositions of stainless steel samples (wt%).

Sample	Si	Mn	Cr	Ni	Fe
1	0.46	0.74	12.35	12.55	73.90
2	0.57	0.791	25.39	20.05	53.20
3	0.21	0.89	14.14	5.66	79.10

5. Results and discussion

Figure 2 shows the full-range spectrum of laser plasma. The spectral detection window of the system was 18 nm. To carry out calculations, it was necessary to record the lines of all elements entering the sample composition. We used several spectral ranges, each containing several spectral lines, chosen to calculate the laser plasma composition (Fig. 3). The spectral parameters of the transitions are given in Table 2.

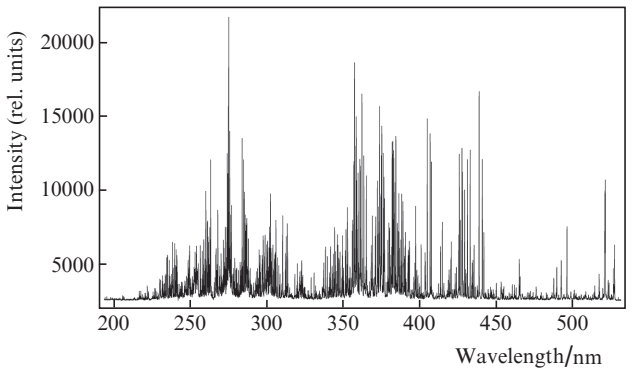

Figure 2. Full-range spectrum of the laser plasma from a steel sample, recorded with an exposure of 5 μs in 2 μs after the end of the laser pulse.

Laser plasma must be optically thin and in local thermodynamic equilibrium to calculate its composition by the CF LIBS. We chose atomic nonresonant lines of the main elements Fe, Ni, and Cr with energies of the lower transition levels exceeding 0.1 eV (Table 2) to check if these requirements are fulfilled. One should expect maximum self-absorption for the atomic transition with the lower level close to the ground level. Generally, the laser plasma temperature is 10000 K for 0.5 μs after the end of the laser pulse; under these conditions, the fractions of atoms with level energies of 3 and

Table 2. Spectral data for the transitions used [see (1)].

Particle	Wavelength/nm	A_{pk}/s^{-1}	E_k/eV	E_p/eV	g_p
Cr I	**396.368**	1.3×10^8	2.54	5.67	15
	396.974	1.2×10^8	2.54	5.67	13
	398.390	1.05×10^8	2.54	5.65	9
	399.110	1.07×10^8	2.54	5.65	7
	433.755	5.48×10^6	0.96	3.83	5
	433.943	6.92×10^6	0.98	3.83	7
	434.450	1.1×10^7	1.00	3.85	9
	435.174	1.2×10^7	1.03	3.88	11
	435.962	5.4×10^6	0.98	3.83	5
	437.126	4.1×10^6	1.00	3.84	7
Fe I	370.556	3.22×10^6	0.052	3.39	7
	370.925	1.56×10^7	0.91	4.25	7
	371.994	1.62×10^7	0	3.33	11
	372.762	2.25×10^7	0.96	4.28	5
	373.486	9.02×10^7	0.85	4.17	11
	373.713	1.41×10^7	0.052	3.36	9
	374.556	1.15×10^7	0.087	3.39	7
	374.589	7.33×10^6	0.12	3.43	3
	374.826	9.15×10^6	0.11	3.41	5
	382.782	1.05×10^8	1.55	4.79	5
	376.554	9.8×10^7	3.23	6.52	15
Fe II	272.754	8.5×10^7	1.04	5.58	4
	273.073	2.5×10^7	1.07	5.61	4
	273.954	1.9×10^8	0.98	5.51	8
	274.638	1.9×10^8	1.07	5.58	6
	276.181	1.1×10^7	1.09	5.58	4
Mn I	**279.482**	3.7×10^8	0.0	4.43	8
	279.827	3.6×10^8	0.0	4.43	6
	280.108	3.7×10^8	0.0	4.42	4
Ni I	**344.625**	4.4×10^7	0.11	3.71	5
	345.289	9.8×10^6	0.10	3.69	7
	345.846	6.1×10^7	0.21	3.79	5
	347.254	1.2×10^7	0.11	3.68	7
	349.295	9.8×10^7	0.10	3.65	3
	351.034	1.2×10^8	0.21	3.74	1
	471.441	4.6×10^7	3.38	6.01	11
Si I	**288.158**	1.89×10^8	0.78	5.08	3

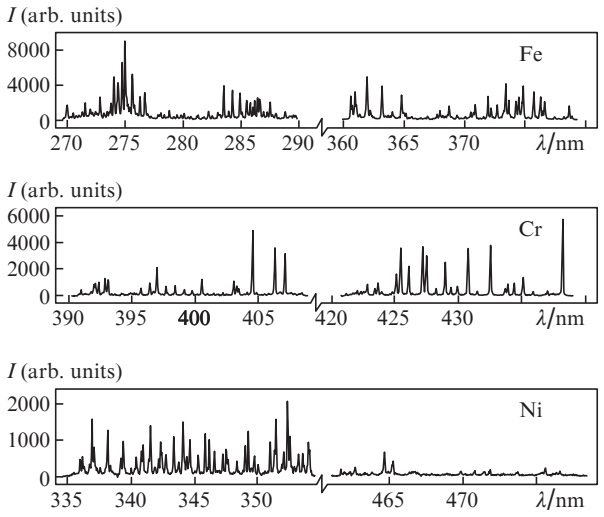

Figure 3. Spectra of Fe, Cr, and Ni in laser plasma (see Table 2), which were used to calculate the plasma composition.

1 eV are, respectively, ~3% and more than 20%. Thus, the self-absorption of radiation for transitions with a lower level energy of 3 eV or more is small even for main elements, and the plasma can be considered as optically thin. Having found the amount of the ath component (n_a) from Eqn (1) for each line under study (the $p-k$ transition) and divided it by the same expression obtained for the transition with the highest lower level energy ($q-w$), one can estimate the degree of self-absorption:

$$\alpha = \left[\frac{I_a^{pk}\lambda_a^{pk}}{A_a^{pk}g_a^{pk}}\exp\left(-\frac{E_a^p}{kT}\right)\right]\left[\frac{I_a^{qw}\lambda_a^{qw}}{A_a^{qw}g_a^{qw}}\exp\left(-\frac{E_a^q}{kT}\right)\right]^{-1}. \qquad (14)$$

If the ($p-k$)-transition line is not self-absorbed in plasma, the α value should be close to unity. The transition for which self-absorption can be neglected was chosen to be the Fe I transition with λ = 376.55 nm and the maximum lower level energy (3.23 eV). As follows from (14), to estimate the degree of self-absorption, one must determine the plasma temperature. It was calculated from the lines of transitions with lower level energies above 1.4 eV. The estimated degrees of self-absorption for the lines of transitions with different lower level energies at different instants are shown in Fig. 4. It can be seen that the Fe I line with λ = 376.56 nm and a lower level energy of 0.05 eV exhibits self-absorption during the first 3 μs, whereas the self-absorption for the Fe I line with λ = 370.9 nm is insignificant. Therefore, the plasma is optically thin for the Fe I lines with a lower level energy exceeding 0.1 eV. Since laser plasma is characterised by a large temperature gradient and density, the strongest self-absorption is expected in its central part. The degree of self-absorption was determined for different lines in different regions of laser plasma and at different distances from the center. According to the data in Fig. 4, the self-absorption for lines with a lower level energy exceeding 0.1 eV depends weakly on the local-region position; i.e., the plasma is optically thin. Similar calculations were performed for Cr and Ni lines, and transitions exhibiting no significant self-absorption were chosen. The self-absorption lines of trace impurities (Mn and Si) can be neglected due to the low concentrations of atoms and ions of these elements in the plasma. The data for the lines that did not undergo self-absorption and were chosen for temperature calculations are bolded in Table 2.

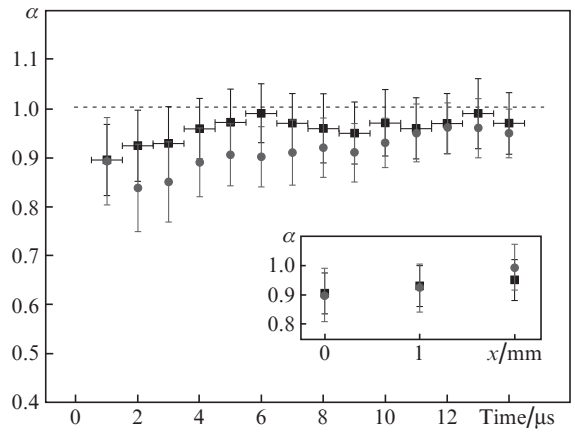

Figure 4. Degrees of self-absorption α (determined with respect to the Fe I line (λ = 376.6 nm) in plasma for the Fe I line at 370.6 nm [lower level at 0.05 eV, (●)] and the Fe I line at 370.9 nm [lower level at 0.9 eV, (■)] during the plasma luminescence. The inset shows the degrees of self-absorption at the center (x = 0) and periphery of the plasma.

The conditions for local thermodynamic equilibrium were verified by comparing the electron temperatures of the plasma calculated from the intensities of spectral lines of different elements. The equality of temperatures at certain instants of plasma evolution indicates that local thermodynamic equilibrium is likely to be implemented. The calculated temperatures for three elements at a chosen evolution instant are shown in Fig. 5a. Figure 6 presents the calculation results for the total time of laser plasma emission. The temperatures calculated from the spectra of Fe, Cr, and Ni atoms coincide, which may be indicative of local thermodynamic equilibrium, which is established 2 μs after the plasma formation onset. The difference in temperatures after 14 μs is likely to be due to the fact that the plasma density decreases and the particle collisions become more rare upon cooling.

The degree of deviation from stoichiometry during laser ablation was calculated by determining the laser plasma composition. Since the emission line intensity rapidly decreases during plasma expansion, we chose the instant when the local thermodynamic equilibrium was established (2 μs after the laser pulse, 2-μs exposure) to record spectra.

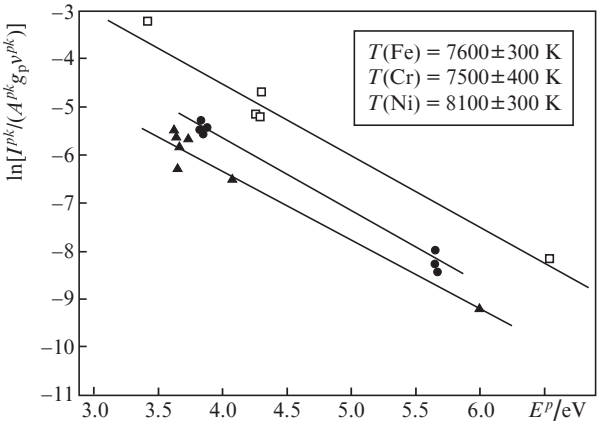

Figure 5. Temperatures calculated for (□) Fe I, (●) Cr I, and (▲) Ni I using the plasma emission spectra recorded with an exposure of 1 μs in 2 μs after the end of the laser pulse.

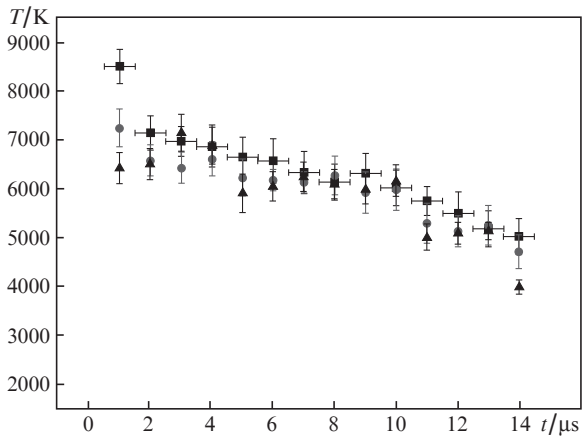

Figure 6. Plasma temperatures calculated from the (■) Fe I, (●) Cr I, and (▲) Ni I lines at different instants during plasma expansion.

Furthermore the CF LIBS was used to calculate the plasma composition for different samples, and the data obtained were compared with the known compositions of the initial alloys. At zero deviation from stoichiometry these compositions should coincide. The results are listed in Table 3, along with the composition calculated taking into account the work function. The W_i values used in the calculations are given in Table 4. As follows from the calculation, selective evaporation is absent for nickel; this result is in agreement with the model proposed, because the W_i values for iron and nickel coincide. At the same time, selective evaporation should manifest itself (to a small extent) for only chromium, since W_i for this element exceeds that for iron by 15%. At chromium concentrations in the sample exceeding 25%, selective evaporation becomes pronounced, and the compositions of the initial sample and plasma differ. When the chromium concentration is reduced to 12%, selective evaporation is absent, and one does not need to correct the work function. The results of calculating the composition within the selective evaporation model are not worse than the results of analysis for chromium; therefore, the consideration of selective evaporation and work function allows one to obtain correct results for

Table 3. Compositions of the initial solid samples and the plasma compositions calculated disregarding and taking into account the work function W_i.

Component	Sample 1			Sample 2			Sample 3		
	Data of Table 1	Calculation disregarding W_i	Calculation taking into account W_i	Data of Table 1	Calculation disregarding W_i	Calculation taking into account W_i	Data of Table 1	Calculation disregarding W_i	Calculation taking into account W_i
Fe	73.9	71.95±6.1	70.38±6.1	53.1	55.45±9.1	53.76±9.1	79.09	79.5±4.3	78.1±4.3
Cr	12.35	12.76±5.22	13.74±5.22	25.39	22.96±5.9	25.59±5.9	14.14	12.76±2.9	15.01±2.9
Ni	12.55	14.19±6.0	14.85±6.0	20.05	20.09±8.1	19.45±8.1	5.66	6.59±3.1	6.18±3.1
Si	0.46	0.50±0.39	0.50±0.39	0.57	0.80±0.39	0.80±0.39	0.23	0.22±0.10	0.22±0.10
Mn	0.74	0.60±0.50	0.51±0.50	0.79	0.70±0.50	0.37±0.50	0.89	0.90±0.30	0.50±0.30

Table 4. Thermophysical parameters for the components of stainless steel samples and the W_i values calculated on their basis.

Component	C_{sol}/J mol^{-1} K^{-1}	T_{melt}/K	ΔH_{melt}/kJ mol^{-1}	C_{fluid}/J mol^{-1} K^{-1}	T_{boil}/K	ΔH_{ev}/kJ mol^{-1}	$W_i/10^{-5}$ J mol^{-1} K^{-1}
Fe	25.1	1811	13.81	46.01	3134	340	8.208
Cr	23.3	2180	21	39.3	2944	339.5	9.482
Ni	26.07	1728	17.48	38.9	3186	377.5	8.460
C	8.5	3773	104.6	8.23	5100	716	32.495
Si	19.8	1687	50.2	27.2	3538	359	8.225
Mn	26.32	1519	12.91	46.01	2173	221	8.631

samples of arbitrary composition. The model proposed can be applied both to samples with a weakly pronounced tendency to deviation from stoichiometry (steels) and to samples exhibiting strong selective evaporation (bronzes); thus, this approach is universal and provides reference-free analysis.

6. Conclusions

It was established that selective evaporation of alloys subjected to laser ablation is caused by the difference in the thermophysical parameters of the sample components. Experimental verification of the degree of deviation from stoichiometry during laser evaporation of high alloy steel samples showed that the manifestation of this effect is rather weak. It was found that selective evaporation occurs for only chromium when its concentration in the sample is about 25%; at lower concentrations chromium exhibits no selective evaporation. It was shown that the proposed model of nonstoichiometric evaporation makes it possible to perform more exact analysis of high alloy steel samples. Our approach correctly describes the selective evaporation during laser ablation of alloys of different types (bronzes, stainless steels), which indicates universality of the model developed.

Acknowledgements. This work was supported by the Russian Foundation for Basic Research (Grant Nos 09-02-01173-a and 11-02-01202-a).

References

1. Cremers D.A., Radziemski L.J. *Handbook of Laser Induced Breakdown Spectroscopy* (England: Wiley, 2006).
2. Prokhorov A.M., Konov V.I., Ursu I., Mikheilesku I.N. *Vzaimodeistvie lazernogo izlucheniya s metallami* (Interaction of Laser Radiation with Metals) (Moscow: Nauka, 1988).
3. Chrisey D.B., Hubler G.K. *Pulsed Laser Deposition of Thin Films* (New York: Wiley, 1994).
4. Phipps C. *Laser Ablation and its Applications* (New York: Springer, 2007).
5. Hahn D., Omenetto N. *Appl. Spectrosc*., **64**, 335A (2010).
6. Pisonero J., Gunther D. *Mass Spectrom. Rev.*, **27**, 609 (2008).
7. Zorov N.B., Gorbatenko A.A., Labutin T.A., Popov A.M. *Spectrochim. Acta, Part B*, **65**, 642 (2010).
8. Nouvellon C., Chaleard C., Lacour J.L., Mauchien P. *Appl. Surf. Sci.*, **138-139**, 306 (1999).
9. Poitrasson F., Mao X., Mao S.S., Freydier R., Russo R.E. *Anal. Chem.*, **75**, 6184 (2003).
10. Pershin S.M., Colao F. *Techn. Phys. Lett.*, **31**, 741 (2005).
11. Liu C., Mao X.L., Mao S.S., Zeng X., Greif R., Russo R.E. *Anal. Chem.*, **76**, 379 (2004).
12. Borisov O.V., Mao X.L., Russo R.E. *Spectrochim. Acta, Part B*, **55**, 1693 (2000).
13. Chan W.T., Russo R.E. *Spectrochim. Acta, Part B*, **46**, 1471 (1991).
14. Russo R.E., Mao X.L., Chan W.T., Bryant M.F., Kinard W.F. *J. Anal. At. Spectrom*., **10**, 295 (1995).
15. Ciussi A., Corsi M., Palleschi V., Rastelli S., Salvetti A., Tognoni E. *Appl. Spectrosc*., **53** (8), 960 (1999).
16. Tognoni E., Cristoforetti G., Legnaioli S., Palleschi V. *Spectrochim. Acta, Part B*, **64** (1), 1 (2010).
17. Ciucci A., Palleschi V., Rastelli S., Salvetti A., Singh D.P., Tognoni E. *Laser Part. Beams*, **17**, 793 (1999).
18. Fornarini L., Colao F., Fantoni R., Lazic V., Spizzicchino V. *Spectrochim. Acta, Part B*, **60**, 1186 (2005).
19. Dudragne L., Adam Ph., Amouroux J. *Appl. Spectrosc.*, **52** (10), 1321 (1998).
20. Lednev V.N., Pershin S.M. *Laser Phys.*, **18**, 850 (2008).
21. Pershin S.M., Colao F., Spizzichino V. *Laser Phys.*, **16**, 455 (2006).
22. Aragon C., Aguilera J.A. *Spectrochim. Acta, Part B*, **63**, 893 (2008).
23. Moon H.-Y., Herrera K.K., Omenetto N., Smith B.W., Winefordner J.D. *Spectrochim. Acta, Part B*, **64**, 702 (2009).
24. El Sherbini M., El Sherbini Th.M., Hegazy H., Cristoforetti G., Legnaioli S., Palleschi V., Pardini L., Salvetti A., Tognoni E. *Spectrochim. Acta, Part B*, **60**, 1573 (2005).
25. Griem H.R. *Plasma Spectroscopy* (London: McGraw-Hill, 1964).
26. Cabalin L.M., Laserna J.J. *Spectrochim. Acta, Part B*, **53**, 723 (1998).
27. Zel'dovich Ya.B., Landau L.D. *Zh. Eksp. Tekh. Fiz.*, **14**, 32 (1944).
28. Kikoin I.K., Senchenkov A.P. *Fiz. Met. Metalloved*., **24**, 843 (1967).
29. Prohorov A.M., Batanov V.A., Bunkin F.V., Fedorov V.B. *IEEE J. Quantum Electron.*, **9** (5), 503 (1973).
30. Fishburn J.M., Withford M.J., Coutts D.W., Piper J.A. *Appl. Opt.*, **43**, 6473 (2004).